DEVELOPMENT AND EVALUATION OF DIRECTIONALLY-SOLIDIFIED NIAL/(CR,MO)-BASED EUTECTIC ALLOYS FOR AIRFOIL APPLICATIONS

S.V. Raj[1], I.E. Locci[2] and J.D. Whittenberger[1]

[1]NASA Glenn Research Center, Cleveland, OH 44135
[2]CWRU at NASA Glenn Research Center, Cleveland, OH 44135

Abstract

The results of recent efforts to develop directionally-solidified alloys based on the Ni-33Al-31Cr-3Mo eutectic composition are discussed. These developmental efforts included studying the effects of macroalloying and growth rates on microstructure formation as well as the elevated temperature compressive and tensile properties of these alloys. These observations revealed that contrary to conventional opinion, the cellular microstructure was stronger and tougher than the planar eutectic microstructure due to a microstructural refinement of the cell size and interlamellar spacing. The high temperature strengths of these alloys are compared with those of commercial superalloys and advanced NiAl single crystals. The implications of this research on airfoil manufacturing and applications are discussed.

Introduction

Although high pressure turbine airfoil vanes were successfully manufactured from a high strength NiAl single crystal alloy and engine tested a few years ago, further developments on this material were not continued owing to the brittleness of the alloy [1,2]. Directionally-solidified (DS) NiAl eutectic alloys have been investigated as alternative materials for airfoil applications due to their higher elevated temperature strength and fracture toughness compared to binary NiAl [3]. Two eutectic systems, namely the NiAl-34(at.%)Cr[1] and the NiAl-9Mo, have been studied in greater detail, where the microstructure consists of either Cr or Mo fibers in a NiAl matrix. These alloy systems offer the possibility that both the creep and the fracture toughness properties can be effectively improved by a combination of alloying and microstructural controls. Thus, several investigators have studied DS NiAl eutectic alloys, where the eutectic phases are ideally parallel to the growth direction, in an effort to optimize the mechanical properties [3–6].

In particular, the Ni-33Al-34Cr [7,8] and the Ni-33Al-(34-x)Cr-xMo [7–14] eutectic alloys, where $0 \le x \le 6\%$, have drawn greater attention since the earlier investigations of Walter and Cline [4–6] demonstrated that the substitution of Mo for Cr leads to a corresponding change in the fiber morphology from Cr rods to (Cr,Mo) lamellar plates when the Mo content exceeds 0.7%. This change in fiber morphology offers the possibility of improved fracture toughness and elevated temperature creep properties.

Conventionally, it has been assumed that these in-situ composites require the two phases to be grown parallel to each other and to the growth direction as a planar eutectic microstructure in order to maximize the mechanical strength in the longitudinal direction. However, planar eutectic microstructures develop in the NiAl/(Cr,Mo) system only when the solidification rate, V_f, is typically less than 25 mm h^{-1} depending on the Mo content of the alloy [5,12,13]. These rates are generally too slow for economic commercial production of any alloy even if it is demonstrated to possess all the requisite properties required for turbine airfoil applications. However, solidification at faster rates leads to the development of cellular eutectic microstructures, where the (Cr,Mo) and the NiAl plates emanate radially from the cell interior to the cell boundaries [12–14]. Cellular microstructures are also likely to form even with small amounts of alloying elements varying between 0.25 and 1% even when V_f is sufficiently slow to produce a planar eutectic microstructure in the

[1]Unless otherwise mentioned, all compositions are reported in atomic percent in this paper.

unalloyed NiAl/(Cr,Mo) material [15]. Clearly, it would be technologically relevant to study the mechanical properties of these cellular microstructures to determine if attractive mechanical properties can be obtained under fast growth conditions.

Historically, cellular microstructures have generally been considered to be undesirable for high temperature structural applications due poor creep properties induced by cell boundary deformation processes. However, growing at faster rates is likely to lead to a refinement in the interlamellar spacing, λ, in accordance with the Jackson-Hunt relationship [16]: $\lambda^2 V_f$ = constant. This relationship has been shown to be valid for the NiAl-34Cr [4] and the Ni-33Al-31Cr-3Mo [13] eutectic alloys with cellular microstructures. Hence, the effect of growth rate on the room temperature fracture toughness and elevated temperature strength is unknown for the NiAl/(Cr,Mo) alloys. Investigations on the effect of withdrawal rates on the microstructures and mechanical properties of these alloys could have important commercial and engineering consequences.

The objectives of this paper are primarily to summarize the results of studies on the effect of macroalloying and growth rate on microstructure formation and elevated temperature properties of directionally-solidified Ni-33Al-31Cr-3Mo alloys. Details of the creep properties of the Ni-33Al-33Cr-1Mo alloy and the effect of growth rate on room temperature fracture toughness will be published separately [18,19].

Background

Statistical design of experiments approach to alloy design

A program to develop directionally-solidified NiAl/(Cr,Mo) eutectic alloys for airfoil applications was initiated at the Glenn Research Center, Cleveland, Ohio, in 1995. It commenced with an attempt to design alloys using a statistical design of experiments (DOE) approach [11,17]. Forty new alloy compositions were formulated by simultaneously and independently varying the compositions of several elements (Al, Cr, Hf, Si, Ta and Ti) in eight-dimensional space based on a DOE model using Ni-33Al-31Cr-3Mo as the base composition. The Mo content was kept constant at 3% while nickel was used as a filler. Duplicate compositions of five of the alloys were also cast in order to comply with the statistical requirements of the DOE model. The elements, Hf, Si, Ta and Ti, were chosen because they were known to improve the high temperature creep strength of NiAl. Since it was impractical to directionally-solidify all these compositions, the alloys were prepared by arc-melting (AM). Their microstructures were qualitatively and quantitatively examined using optical and scanning electron microscopy (SEM) techniques, and the phases were identified by x-ray diffraction (XRD). Details of the alloy compositions, their microstructures and the volume fractions of the individual phases are tabulated in Table I [17]. A close examination of Table I reveals that despite large differences in the compositions of these alloys, the commonly observed microstructures included primary dendrites consisting either of (Cr,Mo), (Cr,Ta) or NiAl phases, and the two- and three-phase eutectic morphologies. The term "other phases" reported in the table includes (Hf,Ti) dendrites, unidentified phases and interdendritic segregation.

The total eutectic volume fraction, V_{total}, given in Table I refers to the summation of the volume fractions of the two- and three-phase eutectic microstructures. Although a complete two-phase, NiAl/(Cr,Mo), or a three-phase, NiAl/(Cr,Mo)/Cr_2Ta, eutectic microstructure was the desired objective for the directional-solidified alloys, these microstructures were not attained when they were processed by arc-melting. For example, the base composition represented by AM-0 revealed an arc-melted microstructure consisting of 92.3% of the two-phase (Cr,Mo)/NiAl eutectic and 7.7% of the primary NiAl dendrites (Table 1) although the NiAl dendrites were usually absent when this alloy was directionally-solidified [10,12,13]. Thus, the volume fractions of the phases are likely to be different if these alloys had been directional-solidified. Duplicate, and in one case triplicate, melts of five of the alloys revealed that the variation in V_{total} was between 0.9 and 8.5%. However, larger variations in the amount of the individual phases were observed in some of the alloys, and in the case of AM-11 and AM-12, some of the phases were not consistently observed despite similarities in their chemical compositions. While noting these limitations of the arc-melting technique for processing the DOE alloys, this method was chosen for its relative simplicity in these early attempts in order to narrow down and identify suitable alloy compositions for directional solidification and detailed study at a later date. The data shown in Table I were used as the input in the DOE model, which was then allowed to predict other alloy compositions with the intention of maximizing the volume fractions of the eutectic microstructures and minimizing other phases. Unfortunately, this approach to alloy design proved to be unsuccessful since the statistical analysis did not give reproducible results presumably due to the wide range of compositions considered and scatter present in the arc melted microstructures. Nevertheless, three compositions predicted by the model were directionally-solidified and their high temperature compressive strength and room temperature fracture toughness were evaluated [11]. Since these alloys were brittle with no significant improvement in their elevated temperature strength, it was concluded that the DOE technique was unsuitable as an alloy design method in the present instance.

Empirical guidelines for alloy design

However, certain insights were gained from the DOE results (Table 1), which formed the basis for designing the next generation alloys. Thus, alloys containing Hf and Si generally tended to promote intercellular segregation, especially when Hf/Ni > 0.025 and Si/Ni > 0.01. Later studies on DS alloys microalloyed with about 0.25% Si confirmed that this element by itself does not promote intercellular segregation [15]. Tantalum tended to promote the formation of three-phase eutectic microstructures when the ratio Ta/Ni > 0.125 although higher Ta/Ni ratios also had a tendency to encourage the precipitation of (Cr,Ta) primary dendrites. For values of Ta/Ni < 0.125, the volume fraction of the intercellular region increased with increasing values of the Ta/Ni ratio. Titanium by itself did not promote intercellular segregation even with a 10% addition (e.g., AM-22 and AM-29) and no precipitates were observed in these alloys. Alloys containing Ti as well as Hf, Si and Ta showed a greater propensity towards intercellular segregation. As a result, Hf and Si were not used in the first generation directionally-solidified alloys although detailed microstructural and mechanical properties studies were later conducted on alloys containing less than 1% of these elements [15]. The total volume fractions of the eutectic microstructures decreased sharply when the Ni content in the alloys deviated more than 3% from the ideal base composition of 33% (Fig. 1(a)) and when the (Al+Cr+Mo+Ta+Ti)/Ni ratio significantly varied from about 2.3 (Fig. 1(b)). These guidelines limited alloy design to a narrow range

Table 1: Compositions of the DOE Alloys in (at.%) and the volume fractions of the phases observed in them.

Code	Ni	Al	Cr	Mo	Ti	Ta	Hf	Si	Total Eutectic	Two-phase Eutectic	Three-phase eutectic	NiAl dendrites	(Cr,Mo) dendrites	(Ta,Cr) dendrites	Intercellular region	Other Phases
AM-0	33.1	33.7	29.3	2.6	0.0	0.0	0.0	0.0	92.3%	92.3%	0.0%	7.7%	0.0%	0.0%	0.0%	0.0%
AM-1	36.3	33.9	26.7	2.9	0.0	0.0	0.0	0.0	71.0%	71.0%	0.0%	29.1%	0.0%	0.0%	0.0%	0.0%
AM-2	32.1	28.6	32.6	2.2	0.0	4.3	0.0	0.0	92.2%	34.8%	57.3%	0.0%	7.0%	0.8%	0.0%	0.0%
AM-3	20.5	34.7	27.6	2.0	9.8	4.4	1.0	0.0	0.0%	0.0%	0.0%	9.8%	46.2%	44.0%	0.0%	0.0%
AM-4	27.9	28.7	27.3	1.7	9.7	4.6	0.0	0.2	70.3%	70.3%	0.0%	0.0%	3.1%	26.6%	0.0%	0.0%
AM-5	24.3	34.4	32.6	2.8	0.0	4.6	1.0	0.4	70.1%	48.7%	21.3%	0.0%	14.3%	15.7%	0.0%	0.0%
AM-6	24.0	26.8	34.8	2.8	10.2	0.0	0.5	0.0	9.5%	9.5%	0.0%	0.0%	78.4%	0.0%	12.1%	0.0%
AM-7	36.4	28.2	26.9	2.3	4.9	0.0	1.0	0.4	76.2%	76.2%	0.0%	0.0%	12.4%	0.0%	11.4%	0.0%
AM-8	25.3	34.6	32.3	2.6	5.1	0.0	0.0	0.2	59.9%	59.9%	0.0%	0.0%	34.1%	0.0%	5.8%	0.0%
AM-9	36.2	28.7	27.2	2.2	0.0	4.6	0.9	0.2	81.4%	16.4%	65.0%	0.0%	0.0%	4.6%	14.0%	0.0%
AM-10	35.4	32.8	29.2	1.5	0.0	0.0	1.0	0.2	81.2%	81.2%	0.0%	11.3%	0.0%	0.0%	5.3%	2.2%
AM-11	31.4	32.7	27.6	2.5	0.0	5.6	0.0	0.1	74.5%	18.9%	55.6%	15.4%	0.0%	10.1%	0.0%	0.0%
AM-12	26.7	26.8	27.8	2.6	9.6	5.4	1.0	0.0	68.0%	68.0%	0.0%	0.0%	0.0%	20.4%	0.0%	11.6%
AM-13	31.8	26.9	27.9	2.6	9.6	0.6	0.5	0.1	71.9%	71.9%	0.0%	0.0%	21.8%	0.0%	6.4%	0.0%
AM-14	24.6	26.3	34.6	2.9	4.5	6.0	0.9	0.1	18.5%	18.5%	0.0%	0.0%	0.0%	69.5%	0.0%	12.0%
AM-15	22.2	30.4	33.8	2.1	9.8	0.6	1.0	0.1	0.0%	0.0%	0.0%	12.9%	50.3%	0.0%	0.0%	36.8%
AM-16	21.5	31.2	36.4	3.3	4.6	2.2	0.9	0.0	23.4%	23.4%	0.0%	0.0%	57.2%	0.0%	19.4%	0.0%
AM-17	29.8	27.2	34.9	2.1	4.9	0.8	0.0	0.0	68.7%	68.7%	0.0%	0.0%	26.3%	0.0%	5.0%	0.0%
AM-18	27.3	33.2	34.2	2.8	0.0	2.4	0.0	0.1	71.5%	71.5%	0.0%	0.0%	14.3%	0.0%	14.2%	0.0%
AM-19	30.2	32.7	33.5	2.9	0.0	0.0	0.5	0.2	80.4%	80.4%	0.0%	0.0%	16.1%	0.0%	3.1%	0.0%
AM-20	20.5	26.7	34.2	2.4	9.4	5.8	1.0	0.0	0.0%	0.0%	0.0%	14.2%	40.9%	31.2%	0.0%	13.6%
AM-21	39.0	26.7	30.8	2.8	0.0	0.6	0.0	0.1	78.9%	78.9%	0.0%	16.6%	0.0%	0.0%	4.5%	0.0%
AM-22	21.0	32.8	34.0	2.6	9.5	0.0	0.0	0.0	13.7%	13.7%	0.0%	0.0%	86.3%	0.0%	0.0%	0.0%
AM-23	26.9	27.0	33.2	3.5	9.2	0.0	0.0	0.1	42.1%	42.1%	0.0%	11.7%	42.1%	0.0%	0.0%	4.2%
AM-24	37.9	26.6	26.2	3.3	0.0	5.8	0.0	0.0	64.1%	22.1%	42.0%	35.9%	0.0%	0.0%	0.0%	0.0%
AM-25	36.1	26.9	33.6	2.1	0.0	0.0	1.0	0.1	66.8%	66.8%	0.0%	9.2%	17.2%	0.0%	6.8%	0.0%
AM-26	25.8	28.2	33.4	2.4	10.2	0.0	0.0	0.1	41.6%	41.6%	0.0%	0.0%	46.3%	0.0%	12.2%	0.0%
AM-27	24.0	35.2	33.5	1.8	0.0	5.6	0.0	0.0	72.0%	37.8%	34.2%	0.0%	14.1%	14.0%	0.0%	0.0%
AM-28	26.9	35.9	33.0	2.3	0.0	0.6	1.1	0.0	68.1%	68.1%	0.0%	0.0%	16.5%	0.0%	15.5%	0.0%
AM-29	30.5	29.5	27.2	2.3	10.5	0.0	0.0	0.0	72.6%	72.6%	0.0%	0.0%	27.4%	0.0%	0.0%	0.0%
AM-30	20.3	27.0	34.1	2.8	10.1	5.0	0.5	0.1	0.0%	0.0%	0.0%	22.0%	41.9%	36.1%	0.0%	0.0%
AM-31	24.0	35.4	27.2	1.9	10.7	0.0	1.1	0.0	23.4%	23.4%	0.0%	18.1%	31.6%	0.0%	26.9%	0.0%
AM-32	28.1	35.3	27.7	2.3	0.0	5.5	1.0	0.0	58.6%	58.6%	0.0%	14.7%	0.0%	26.7%	0.0%	0.0%
AM-33	19.7	35.5	26.9	2.4	10.5	5.2	0.0	0.0	5.1%	5.1%	0.0%	60.6%	0.0%	34.3%	0.0%	0.0%
AM-34	36.1	29.5	30.9	2.4	0.0	0.0	1.0	0.0	83.8%	83.8%	0.0%	8.3%	0.0%	0.0%	7.9%	0.0%
AM-35	22.8	30.1	28.1	2.7	10.4	4.8	1.0	0.2	20.9%	20.9%	0.0%	16.0%	0.0%	33.3%	0.0%	29.7%
AM-36	38.7	30.3	28.3	2.6	0.0	0.0	0.0	0.1	67.4%	67.4%	0.0%	32.6%	0.0%	0.0%	0.0%	0.0%
AM-37	34.1	29.2	33.2	2.3	0.0	0.6	0.6	0.0	71.0%	71.0%	0.0%	3.2%	12.1%	0.0%	13.8%	0.0%
AM-38	37.7	29.0	27.5	2.6	0.0	2.1	1.1	0.0	48.6%	48.6%	0.0%	22.5%	0.0%	0.0%	28.9%	0.0%
AM-39	22.9	28.8	35.3	2.8	4.9	5.2	0.0	0.2	14.7%	14.7%	0.0%	11.7%	51.3%	22.4%	0.0%	0.0%
AM-40	28.6	30.5	31.0	2.8	4.8	1.8	0.5	0.0	37.4%	37.4%	0.0%	9.2%	40.1%	0.0%	13.3%	0.0%

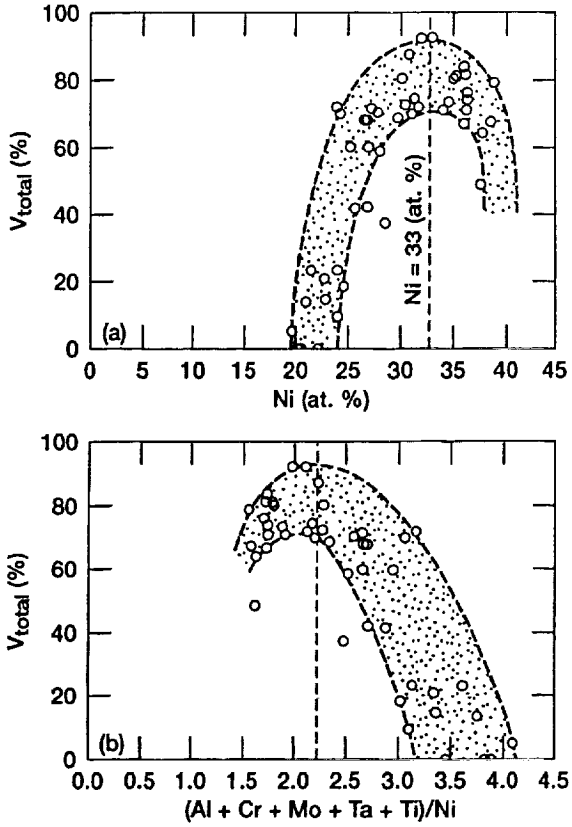

Figure 1.—Variation of the total volume fraction of the eutectic phases in the DOE alloys with (a) nickel content and (b) the ratio (Al + Cr + Mo + Ta + Ti)/Ni.

around the base composition, AM-0, in order to maximize the volume fraction of the eutectic microstructure.

The following selection criteria were developed to narrow the list of alloy compositions for directional solidification and detailed microstructural and mechanical property studies. First, alloys with a total eutectic content less than 70% were dropped from consideration. Second, alloys containing significant amounts of (Cr,Ta) dendrites or those showing intercellular segregation were deleted from the selection list since it was felt that these alloys could not be effectively toughened. Third, alloys containing significant amounts of NiAl dendrites were not considered owing to possible detrimental effects on high temperature creep properties. However, alloys AM-2 and AM-29, which consisted primarily of the eutectic and (Cr,Mo) dendritic microstructures, showed promise for further development. It was felt that the small amounts of (Cr,Ta) dendrites observed in AM-2 could be suppressed with either small modifications to its composition or by directional solidification. Thus, two new alloys were designed and directionally-solidified: NASA-2.1 with a nominal composition of Ni-33Al-29Cr-2Ta, and NASA-29.1 with a nominal composition of Ni-32.5Al-29Cr-3Mo-3Ti. In order to maintain consistency, directionally-solidified base composition, Ni-33Al-31Cr-3Mo, is designated as NASA-0 in this paper.

Experimental Procedures

Details of the DS technique, the test methods used for determining the constant engineering strain rate and constant load creep properties, and the chemical compositions of the alloys have been described elsewhere [10–15,18,19] and only a brief description is included in this paper. Induction-melted rods of selected alloy compositions were directionally-solidified by a modified Bridgman method under a temperature gradient of 8–10 K mm^{-1}. The variations in chemical composition and microstructures of the base composition were found to be within acceptable limits both along the length of DS zone (~100 mm) as well as from one batch to another for rods grown at 12.7 mm h^{-1} [10]. Three alloys, NASA-0, NASA-2.1 and NASA-29.1, were processed at this growth rate. Having established the ability to directionally solidify the base eutectic alloy rods in a reproducible manner at a single growth rate of 12.7 mm h^{-1}, additional rods of the Ni-33Al-33Cr-1Mo (NASA-0.1) and the Ni-33Al-31Cr-3Mo (NASA-0) eutectic alloys were grown at rates varying between 7.6 and 508 mm h^{-1}. The DS rods were sectioned for chemical and metallographic analyses as well as for the machining of creep and fracture toughness specimens as described elsewhere [10,12,13]. Optical and scanning electron microscopy (SEM) and back-scattered electron (BSE) imaging techniques were employed for microstructural observation. In addition, x-ray diffraction (XRD) and energy dispersive spectroscopy (EDS) analysis was used for phase identification.

The long axis of the creep specimens were parallel to the growth direction. Compression specimens were 8 x 4 x 4 mm in size while tensile specimens had a rectangular cross-section of 3.2 x 2.2 mm and a gage length of 25.4 mm. Ridges, which were machined on the tensile creep specimens to permit the attachment of an extensometer, allowed the gage length to be precisely determined. The as-cast EDM layers were removed by grinding the surfaces on 600 grit SiC paper. Constant engineering strain rate and constant load creep tests were conducted in air between absolute temperatures, T, 1100 and 1400 K under engineering strain rates, $\dot{\epsilon}$, varying between 2×10^{-7} and 2×10^{-4} s^{-1} and initial stresses, σ, varying between 30 and 200 MPa, respectively [10,14,15]. The tensile creep properties compared reasonably well with compression data obtained by constant load compression creep and constant engineering strain rate techniques [10]. Thus, it was possible to determine the elevated temperature strength of these alloys by conducting compression tests which allowed more specimens to be tested from a single DS rod.

Results and Discussion

Microstructures

The DS eutectic microstructures observed in both NASA-0.1 and NASA-0 alloys were dependent on the growth velocity. Examples of planar eutectic microstructures observed on transverse sections of NASA-0.1 and NASA-0 are shown in Figs. 2(a) and (b), respectively. The dark and light phases observed in these microstructures are NiAl and (Cr,Mo), respectively. Additional details pertaining to qualitative and quantitative descriptions of these microstructures are discussed elsewhere [13,14,18]. Planar eutectic microstructures, which formed only when $V_f \leq 12.7$ mm h^{-1}, consisted of alternating parallel plates of the (Cr,Mo) and NiAl phases within each eutectic colony. Although both alloys had similar microstructures at these slow growth rates, faceted (Cr,Mo) rods were sometimes observed in the Ni-33Al-33Cr-1Mo alloy. At growth rates exceeding 12.7 mm h^{-1}, the microstructure changed from planar eutectic colonies to cells, where the (Cr,Mo) and the NiAl plates emanated radially from the cell interior

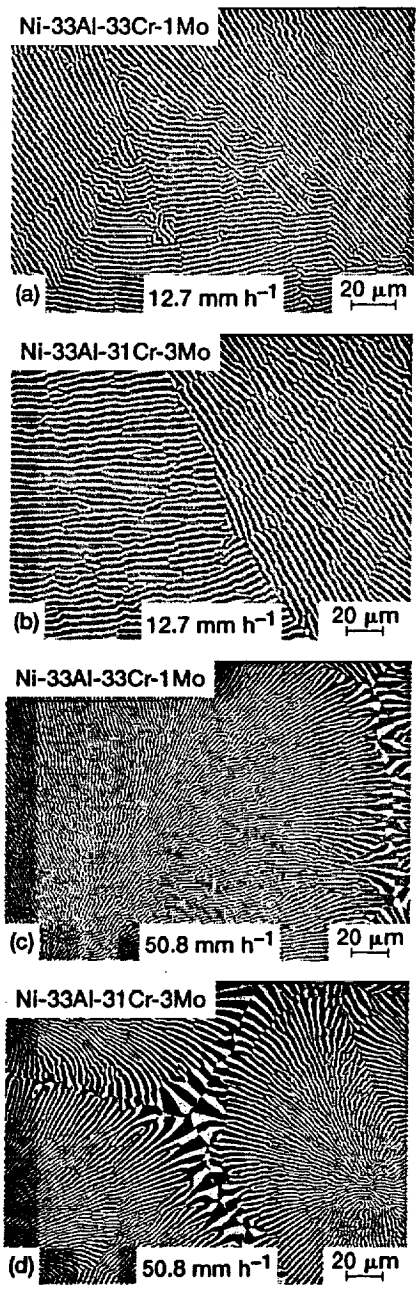

Figure 2.—Optical microstructures of NASA-0 and NASA-0.1 alloys directionally solidified at (a) and (b) 12.7 mm h^{-1} and (c) and (d) 50.8 mm h^{-1}. Micrographs (a) and (c) represent NASA-0.1 while (b) and (d) are for NASA-0.

to the cell boundaries (Fig. 2(c) and (d)). In comparison to the planar eutectic microstructures, where the width of the colony boundaries were narrow and often indiscernible, the average width of the cell boundary varied between 20 and 25 μm irrespective of growth speed [13]. Microstructural observations of longitudinal sections of these alloys revealed that the eutectic grains were several millimeters long for the both the cellular and planar morphologies but the orientation of the lamellae were not always parallel to the growth direction. The microstructures observed in NASA-0.1 and NASA-0 were similar at growth speeds ≤ 254 mm h^{-1}, although there were regions adjacent to the cell boundaries in the NASA-0.1 alloy, where the (Cr,Mo) phase had broken down into particulates. However, an important difference was observed in the microstructures of these two alloys at a growth speed of 508 mm h^{-1}, where the (Cr,Mo) phase had broken down into short plates in the NASA-0.1 alloy. In contrast, the NASA-0 alloy had long (Cr,Mo) plates extending the entire length of the cell.

Figures 3(a) and (b) show the longitudinal and transverse sections of alloy NASA-2.1 containing Ta, respectively, while Figs. 3(c) and (d) show the corresponding microstructures for the Ti-containing NASA-29.1 alloy. Both these alloys were grown at 12.7 mm h^{-1}. In comparison to the planar eutectic microstructure observed in NASA-0 grown at this speed (Fig. 2(b)), NASA-2.1 exhibited a coarse cellular eutectic microstructure consisting of broken (Cr,Mo) platelets (light gray phase in Fig. 3(a)) and primary NiAl dendrites (Fig. 3(b)). In addition, the Cr_2Ta laves phase was also observed in this alloy (white phase in Fig. 3(a)). Low magnification observations of longitudinal sections of NASA-29.1 showed a banded microstructure consisting of alternating regions of coarse and fine (Cr, Mo) lamellae [10]. The transverse sections showed that the microstructure had a cellular morphology (Fig. 3(d)) with an internal microstructure consisting only of (Cr,Mo) and NiAl(Ti) phases (Fig. 3(c)).

Elevated Temperature Deformation Properties

The creep properties of the NASA-0.1 alloy are described in great detail elsewhere [14,19] and will not be discussed here. In the early experiments conducted to determine batch-to-batch variations in chemical composition, microstructures and elevated temperature strength of the NASA-0 alloy grown at a constant growth speed of 12.7 mm h^{-1}, it was observed that some batches contained regions with NiAl dendrites (Figs. 4(a) and (b)). The presence of these dendrites were detrimental to creep properties as shown in Figs. 5(a) and (b), which show plots of true tensile creep strain, ε, versus time, t, and tensile $\dot{\varepsilon}$ versus ε, respectively, at 1300 K under an tensile engineering stress of 50 MPa. It is clear from Fig. 5 that batch 11/96 was considerably weaker than batch 12/96 due to the presence of NiAl dendrites in the microstructure (Figs. 4(a) and (b)). However, with further refinement in the processing technique, microstructural observations on later batches of material did not reveal any NiAl dendrites. Figure 5 also compares the constant load tensile creep curves for NASA-0 with those for NASA-2.1 and NASA-29.1. These three alloys exhibit a short normal primary transient, where the creep rate decreases sharply with increasing creep strain to a minimum value before continuing to increase to final rupture (Fig. 5(b)). For the creep conditions shown in Fig. 5, the Ta-containing NASA-2.1 was stronger than both the base composition NASA-0 as well as the Ti-containing NASA-29.1 below $\approx$ < 7%. However, under higher stresses and lower temperatures, NASA-29.1 was observed to be comparable or stronger than NASA-0 and NASA-2.1 and the creep properties of the latter alloy were comparable to NASA-0 [10].

Figures 6(a) and (b) confirm that directional solidification results in an improvement in the elevated temperature strength of the NASA-0 alloy for both the planar (Fig. 6(a)) and cellular (Fig. 6(b)) eutectic microstructures, where the specimens were grown at 12.7 and 50.8 mm h^{-1}, respectively, with the strengthening effect being greater at the lower temperatures. The strain rate exhibits a change from a power-law to an exponential dependence with increasing stress for

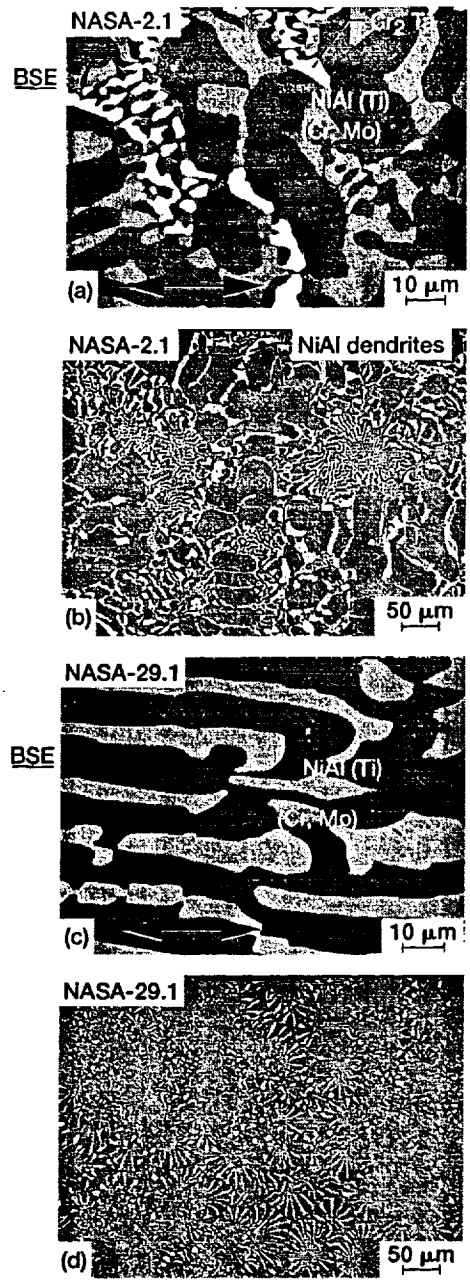

Figure 3.—(a) Back-scattered electron image and (b) optical micrograph of longitudinal and transverse sections of Ni-33Al-29Cr-3Mo-2Ta, respectively; (c) back-scattered electron image and (b) optical micrograph of longitudinal and transverse sections of Ni-32.5Al-29Cr-3Mo-3Ti, respectively.

the as-cast specimens at all temperatures. A similar dependence is also observed at all temperatures for the planar eutectic microstructure (Fig. 6(a)), and at 1200 and 1300 K for the cellular microstructures (Fig. 6(b)). However, the cellular microstructures exhibit a power-law dependence at 1400 K (Fig. 6(b)). A multiple regression analysis of the intermediate and low stress data assuming a power-law stress dependence suggested that the activation energy for deformation, Q_c, was 372.3 ± 29.6 kJ mol^{-1} for the as-cast material, where the error

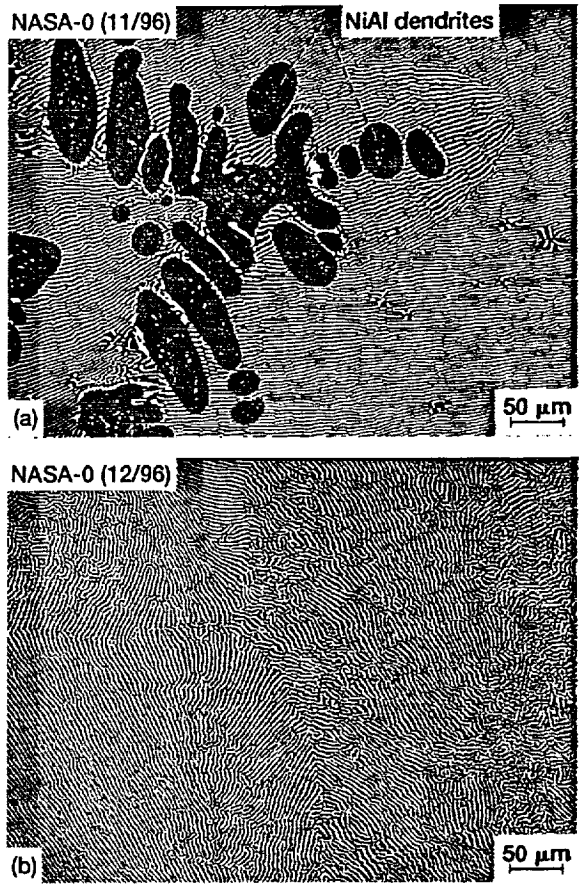

Figure 4.—Comparison of the transverse optical microstructures of two batches of Ni-33Al-31Cr-3Mo directionally solidified at 12.7 mm h^{-1}; (a) DS run 11/96 and (b) DS run 12/96.

values represent one standard deviation about the mean, and varied between 405.1 ± 29.9 and 539.4 ± 24.3 kJ mol^{-1} for the directionally-solidified specimens. The corresponding stress exponents, n, were 4.6 ± 0.2 for the as-cast materials and varied between 4.4 ± 0.2 and 5.6 ± 0.2 for the DS alloys. The growth rate did not appear to influence the activation energy in any consistent manner thereby indicating that the deformation mechanism was independent of the DS microstructure. Nevertheless, the magnitudes of Q_c for the DS materials are generally higher than those reported for polycrystalline high purity Cr for which $Q_c \approx 305$ kJ mol^{-1} in a similar range of temperature [20]. Although the magnitudes of Q_c for the as-cast DS alloys are closer to the values of 440 and 455 kJ mol^{-1} reported for NiAl <001> single crystals [21], it cannot be unambiguously concluded that deformation of the NiAl phase controls the deformation of the eutectic alloys.

Figures 7 (a) and (b) show the variation of the creep rate with stress for NASA-2.1 and NASA-29.1, respectively, in the temperature range 1100 to 1400 K. The data include compression and tension results from several batches [10]. The stress exponent varies between 5.7 and 6.0 for NASA-2.1 while it varies between 3.8 and 4.4 for NASA-29.1. Multiple regression analysis of the data for these alloys assuming a power-law stress dependence revealed that $n \approx 5.5 \pm 0.2$ and $Q_c \approx 419.3 \pm 21.8$ kJ mol^{-1} for NASA-2.1 and $n \approx 4.1 \pm 0.2$ and $Q_c \approx 529.7 \pm 25.8$ kJ mol^{-1} for NASA-29.1. Once again, no deep

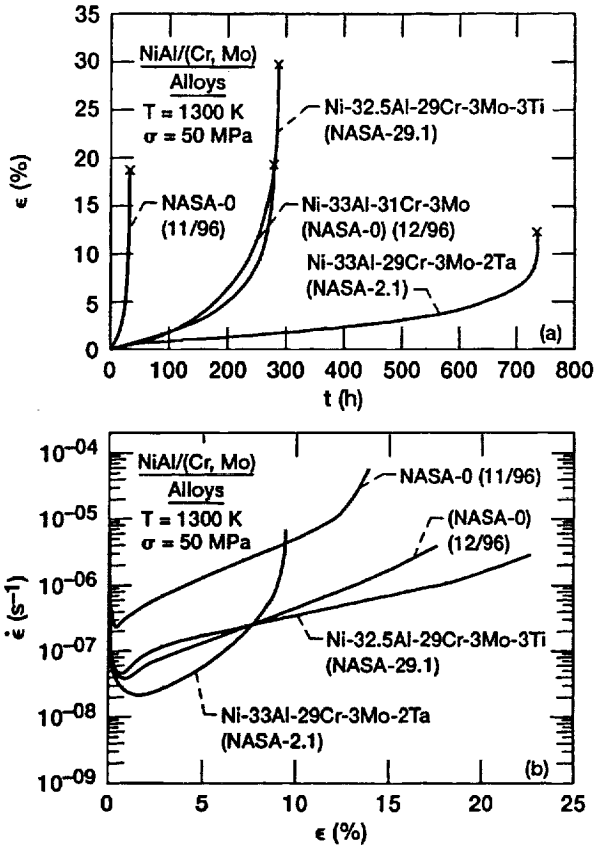

Figure 5.—(a) True tensile creep strain vs. time and (b) true tensile creep rates vs. true creep strain plots for two batches of NASA-0, NASA-2.1 and NASA-29.1.

insights can be gained from these values of n and Q_c except that they suggest that the deformation mechanisms operating in these two alloys at these temperatures are probably similar to those acting in NASA-0.

Figure 8 compares the compressive and tension creep strength for different batches of NASA-0, NASA-2.1 and NASA-29.1 with those for polycrystalline NiAl [22], DS Ni-33Al-28Cr-6Mo [7], cryomilled NiAl-30.4% AlN [23] and NASAIR 100 superalloy single crystals [24]. The data for NiAl, Ni-33Al-28Cr-6Mo and NiAl-30.4% AlN represent compressive properties at 1300 K while those for NASAIR were determined by tensile creep at 1273 K. Several points may be noted from Fig. 8. First, the DS alloys are much stronger than binary NiAl. Second, the compression and tension data are comparable although there is significant scatter in the data. Third, there is no advantage in alloying NASA-0 either with Ta or Ti since there was no effective improvement in the elevated temperature strength. Fourth, the DS alloys are much weaker than cryomilled NiAl-30.4% AlN and NASAIR 100 superalloy single crystals. Furthermore, our studies have also revealed that many other alloying elements even when added in small amounts effectively destroy the initially planar microstructure without any significant improvements in the high temperature strength [15]. These results suggest that macro- and microalloying of NASA-0 is unlikely to be an effective method for improving its elevated temperature strength under the DS conditions used in the present study.

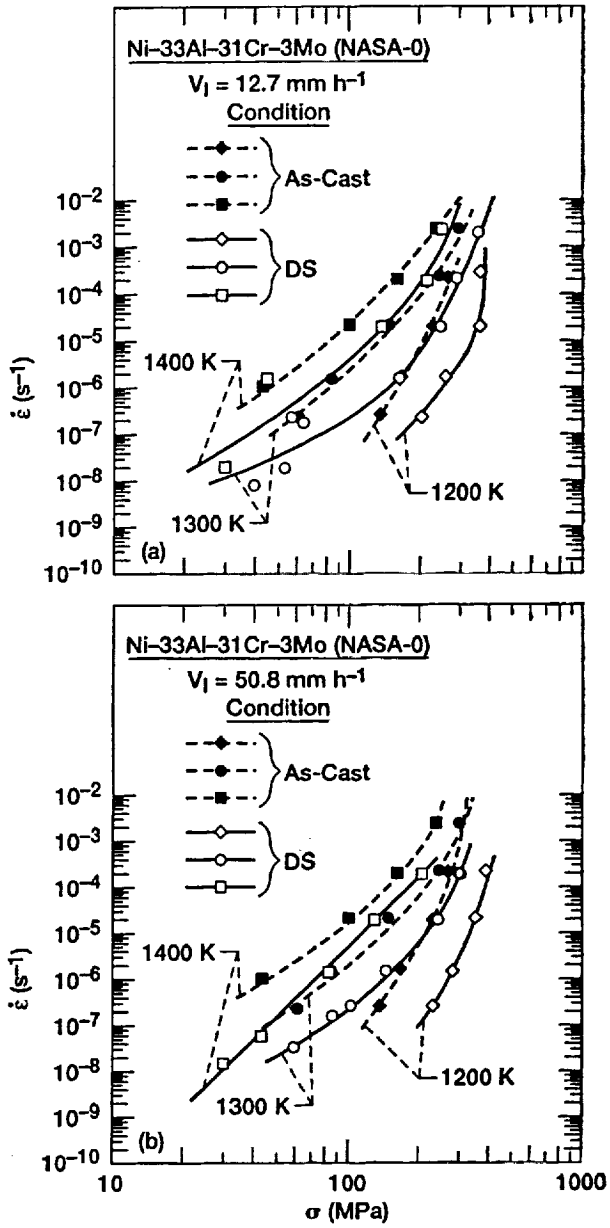

Figure 6.—Comparison of the compressive true strain rate vs. compressive true stress plots for as-cast (solid symbols) and DS (open symbols) NASA-0 grown at (a) 12.7 and (b) 50.8 mm h^{-1} between 1200 and 1400 K.

Effect of Growth Rate on Elevated Temperature Strength

In the absence of a suitable alloying scheme for improving the elevated temperature strength of NASA-0, one possibility was to verify if microstructural refinement would result in any strengthening effects. Two ways in which this refinement can be achieved is by significantly increasing the thermal gradient of the equipment and by withdrawing the DS ingots at higher speeds. Since the thermal gradient of the equipment could not be increased without a major modification of its design, microstructural refinement was achieved by increasing the growth speed (Fig. 2) [13]. Figure 9 shows the effect

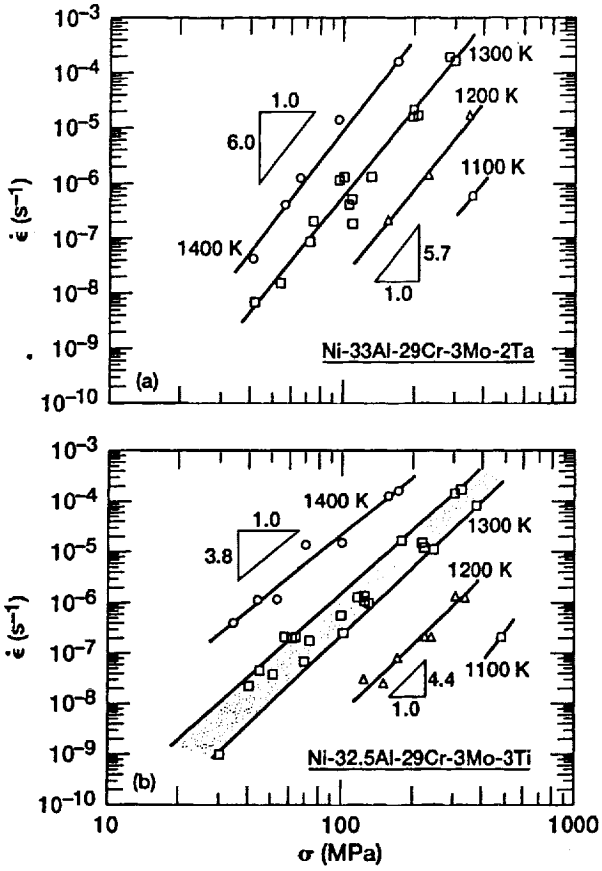

Figure 7.—Strain rate vs. stress data for directionally solidified (a) NASA-2.1 and (b) NASA-29.1 between 1100 and 1400 K.

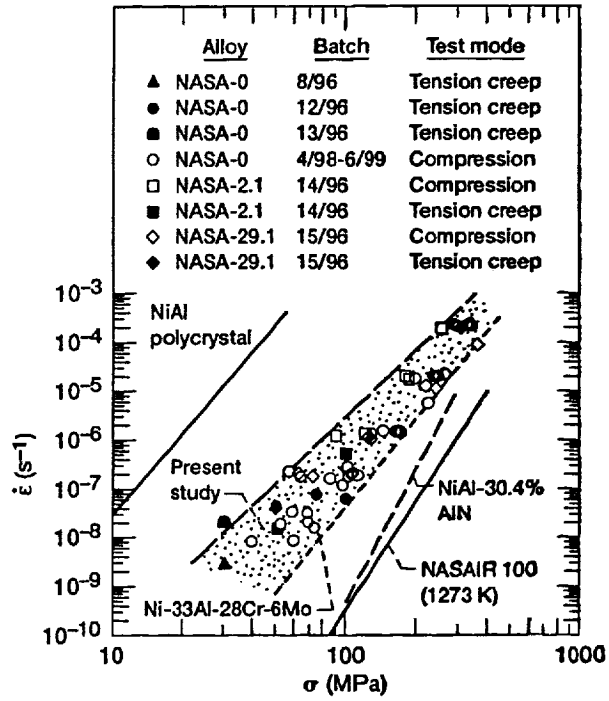

Figure 8.—Comparison of the elevated temperature strengths of the DS NASA-0, NASA-2.1 and NASA-29.1 at 1300 K with those for NASAIR 100 single crystals [24], binary powder-metallurgy extruded NiAl polycrystals [22], DS Ni-33Al-28Cr-6Mo [7] and cryomilled NiAl-30.4% AlN [23].

of growth rate on the elevated temperature strength at approximately 1300 K for < 10^{-4} s^{-1} (Fig. 9(a)) and room temperature fracture toughness, K_p (Fig. 9(b)) [18] as the microstructure changes from a planar eutectic to a radial cellular eutectic microstructure for Ni-33Al-34Cr [4], Ni-33Al-33Cr-1Mo and Ni-33Al-31Cr-3Mo with increasing growth rate. All three alloys show an increase in strength (Fig. 9(a) and toughness (Fig. 9(b)) as V_f increases from 7.6 to 50.8 mm h^{-1}. However, Ni-33Al-33Cr-1Mo loses its strength as well as its toughness as the growth rate increases above 50.8 mm h^{-1}. In contrast, Ni-33Al-31Cr-3Mo continues to increase in strength while retaining its room temperature toughness at higher growth rates. This observation demonstrates that it is possible to improve both the elevated temperature strength as well as the room temperature fracture toughness for some NiAl eutectic alloys by directionally solidifying them at faster growth rates. Although the current generation of alloys are still weaker than the first generation superalloy single crystals (Fig. 8), the observations in Fig. 9 demonstrate that it may be commercially feasible to directionally solidify future generations of new NiAl eutectic alloys at fast enough growth rates without a significant deterioration in their mechanical properties.

The strength of NASA-0 at 1300 K was observed to increase with increasing V_f only at strain rates above 10^{-5} s^{-1} (Fig. 10(a)). Similar observations were made at 1200 K. However, the growth rate had no effect on the elevated temperature strength when the strain rate was about 10^{-6} s^{-1} or at 1400 K for $\dot{\epsilon}$ varying between 10^{-6} and 10^{-4} s^{-1}.

It is likely that the elevated temperature strength of NASA-0 decreases in a manner similar to the observations on Ni-33Al-34Cr [4] and Ni-33Al-33Cr-1Mo (Fig. 9(a)). Correlations of the strength observed at 1300 K with the average cell size, $\bar{d}$, (Fig. 10(b)) and interlamellar spacing, $\bar{\lambda}$, (Fig. 10(c)) suggest that microstructural refinement is effective only at strain rates greater than 10^{-6} s^{-1}. It is clear from Figs. 10(b) and (c) that both $\bar{d}$ and $\bar{\lambda}$ influence the magnitude of the elevated strength at 1300 K. Since there is a correlation between $\bar{d}$ and $\bar{\lambda}$ [13], the similar dependencies shown in Figs. 10(b) and (c) is to be expected. Nevertheless, Figs. 10(b) and (c) clearly demonstrate that microstructural refinement due to an increase in the growth speed can only lead to limited improvements in the elevated temperature strength. Further microstructural refinements leading to a significant decrease in $\bar{\lambda}$ will require the thermal gradients to be increased by factors of two or more using either the edge-defined film (EDF) growth technique, fluidized bed or molten metal cooling technology. This conclusion is consistent with the limited tensile data published by Yang *et al.* [9] on EDF grown Ni-33Al-33Cr-1Mo alloy, where its strength at 1273 K is comparable to that of NASAIR 100 [24] if it is superposed on Fig. 8.

Larson-Miller Plots

Figures 11(a) and (b) compares the variation of the applied tensile creep stress and the density-compensated tensile creep stress with the Larsen-Miller parameter (LMP) [25], T(log t_f + 20), where t_f is the creep rupture time in h, respectively, for several current and potential airfoil alloys. The commonly assumed value of 20 for the LMP

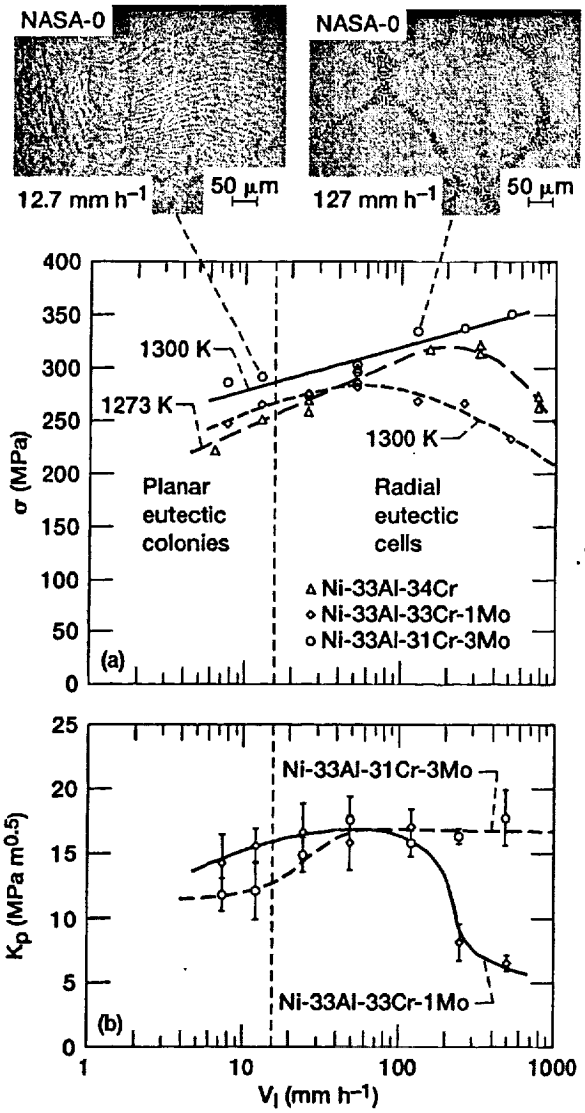

Figure 9.—Variation in (a) the strength at 1273 or 1300 K and (b) the room temperature fracture toughness [18] with growth rate for NiAl-34Cr [4], NASA-0 and NASA-0.1. The representative microstructures at the low and high growth rates are also shown.

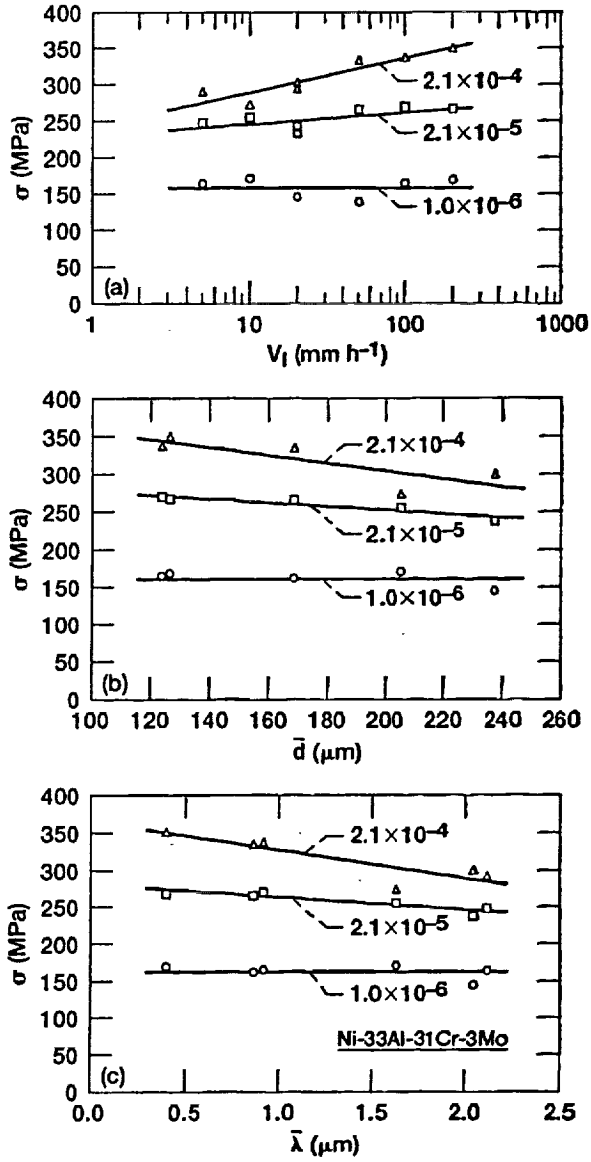

Figure 10.—Effect of (a) growth rate, (b) average cell size and (c) average interlamellar spacing on the compressive strength of NASA-0 at 1300 K under engineering strain rates varying between 10^{-6} and 2.1×10^{-4} s^{-1}.

constant has been used in the construction of these plots. The data for the DS NiAl eutectic alloys were obtained from several batches of the first generation NASA-0, NASA-2.1 and NASA-29.1 alloys whereas the data for NiAl polycrystal, advanced superalloys and NiAl single crystal alloys were obtained from the literature [26]. On an absolute scale, the limited data for these first generation alloys reveal that they are weaker than the commercial superalloys and the advanced NiAl single crystal alloys (Fig. 11(a)). However, their density-compensated tensile creep strengths are comparable to those of polycrystalline René 80 at the upper end of the scatter plot when LMP > 29 x 10^3 (K). Since macroalloying and microalloying [15] have not proven very effective in increasing the elevated temperature strengths of these alloys, the only viable option for improving their creep properties appears to be through microstructural refinement. Since strength generally scales as $1/\bar{\lambda}$, it remains to be demonstrated whether a reduction in the interlamellar spacing by a combination of increased growth speed and thermal gradient during directional solidification would result in significantly creep-resistant alloys.

Summary and Conclusions

The results of a systematic research program undertaken to develop directionally solidified NiAl eutectic alloys based on the Ni-33Al-31Cr-3Mo (NASA-0) composition are discussed. Initial attempts to develop alloys using a statistical design of experiments approach on arc-melted compositions proved to be unsuccessful. The microstructures of two new alloys, Ni-33Al-29Cr-2Ta (NASA-2.1) and Ni-32.5Al-29Cr-3Mo-3Ti (NASA-29.1), resulted in the formation of coarse cellular microstructures. The creep properties of these alloys were not much better than the base alloy. These results taken together with the microstructural observations from the DOE study

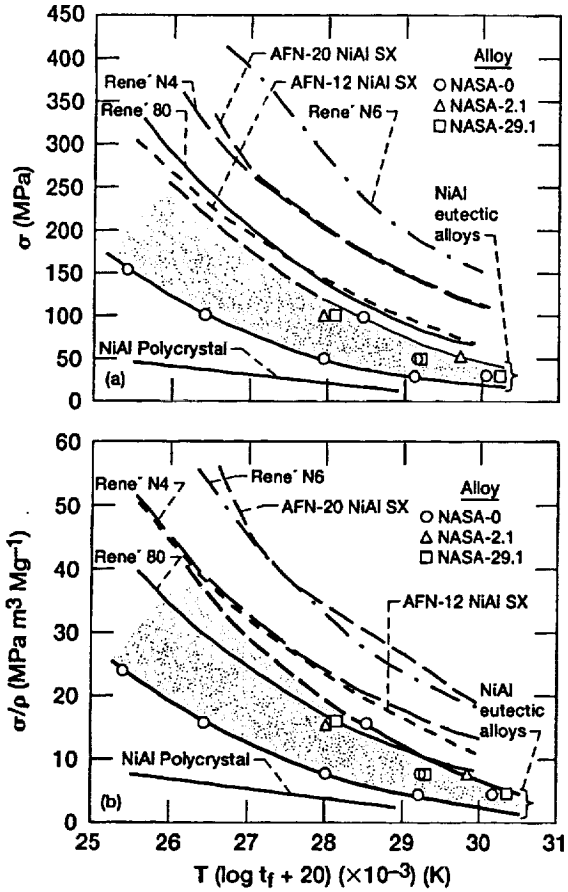

Figure 11.—Comparison of the (a) Larson-Miller and (b) density-compensated Larsen-Miller plots for DS NASA-0, NASA-2.1 and NASA-29.1 with those for current and potential airfoil materials [26].

suggest that macroalloying of NASA-0 is unlikely to improve its creep properties. Studies on improving the elevated temperature strength of NASA-0 by microstructural refinement due to high growth rates proved to be somewhat more successful without any deterioration in the room temperature fracture toughness properties. These observations clearly demonstrate that it is possible to improve both the elevated temperature creep properties and room temperature fracture toughness of this alloy simply by increasing the growth velocity during directional solidification. Thus, DS can be a commercially viable manufacturing technique for making airfoils from NiAl eutectic alloys.

References

1. R.D. Noebe and W.S. Walston, *Structural Intermetallics 1997 (ISSI-2)*, edited by M.V. Nathal, R. Darolia, C.T. Liu, P.L. Martin, D.B. Miracle, R. Wagner and M. Yamaguchi, The Minerals, Metals & Materials Society, Warrendale, PA, pp. 573–84 (1997).
2. W.S. Walston and R. Darolia, *Structural Intermetallics 1997 (ISSI-2)*, edited by M.V. Nathal, R. Darolia, C.T. Liu, P.L. Martin, D.B. Miracle, R. Wagner and M. Yamaguchi, The Minerals, Metals & Materials Society, Warrendale, PA, pp. 573–84 (1997).
3. J.M. Yang, *JOM* 1997; 49: 40.
4. J.L. Walter and H.E. Cline, *Metall. Trans.* **1**, 1221 (1970).
5. H.E. Cline and J.L. Walter, *Metall. Trans.* **1**, 2907 (1970).
6. H.E. Cline, J.L. Walter, E. Lifshin and R.R. Russell. *Metall. Trans.* 2, 189 (1971).
7. D.R. Johnson, X.F. Chen, B.F. Oliver, R.D. Noebe and J.D. Whittenberger, *Intermetallics* **3**, 99 (1995).
8. T.M. Pollock and D. Kolluru, *Micromechanics of Advanced Materials: A Symposium in Honor of Professor James' Li's 70th Birthday*, edited by S.N.G. Chu, P.K. Liaw, R.J. Arsenault, K. Sadananda, K.S. Chan, W.W. Gerberich, C.C. Chau and T.M. Kung, The Minerals, Metals & Materials Society, Warrendale, PA, pp. 205–12 (1995).
9. J.M. Yang, S.M. Jeng, K. Bain and R.A. Amato, *Acta Mater.* **45**, 295 (1997).
10. S.V. Raj, I.E. Locci and J.D. Whittenberger, *Creep Behavior of Advanced Materials for the 21st Century*, edited by R.S. Mishra, A.K. Mukherjee and K. Linga Murty, The Minerals, Metals & Materials Society, Warrendale, PA, pp. 295–310 (1999).
11. I.E. Locci, S.V. Raj, J.D. Whittenberger, J.A. Salem and D.J. Keller, *High-Temperature Ordered Intermetallic Alloys—VIII, Vol.* 552, edited by E.P. George, M. Yamaguchi and M. J. Mills, Materials Research Society, Pittsburgh, PA, pp. KK8.1.1 (1999).
12. J.D. Whittenberger, S.V. Raj, I.E. Locci and J.A. Salem, *Intermetallics* **7**, 1159 (1999).
13. S.V. Raj and I.E. Locci, *Intermetallics*, **9**, 217 (2001).
14. J.D. Whittenberger, S.V. Raj and I.E. Locci, *High-Temperature Ordered Intermetallic Alloys—IX*, **Vol. 646**, edited by J.H. Schneibel, R.D. Noebe, S. Hanada, K.J. Hemker and G. Sauthoff, Materials Research Society, Pittsburgh, PA, N 6.9 (2001).
15. J.D. Whittenberger, S.V. Raj, I.E. Locci and J.A. Salem, this volume.
16. K.A. Jackson and J.D. Hunt, Trans AIME **236**, 1129 (1966).
17. S.V. Raj, I.E. Locci, P. Dickerson, R.D. Noebe, M.V. Nathal and D.J. Keller, unpublished research, Glenn Research Center, 1996.
18. S.V. Raj, I.E. Locci, J.A. Salem and R. Pawlik, to be published.
19. J.D. Whittenberger, S.V. Raj, I.E. Locci and J.A. Salem, to be published.
20. J.R. Stephens and W. Klopp, J. Less Com. Metals **27**, 87 (1972).
21. J.D. Whittenberger and R.D. Noebe, unpublished research, Glenn Research Center, Cleveland, Ohio (1990).
22. S.V. Raj and S.C. Farmer, Metall. Trans. **26A**, 343 (1995).
23. M.G. Hebsur, J.D. Whittenberger and A. Garg, *Structural Intermetallics—1997 (ISSI-2)*, edited by M.V. Nathal, R. Darolia, C.T. Liu, P.L. Martin, D.B. Miracle, R. Wagner and M. Yamaguchi, The Minerals, Metals & Materials Society, Warrendale, PA, pp. 621–630 (1997).
24. M.V. Nathal and L.J. Ebert, Metall. Trans. **16A**, 427 (1985).
25. F.R. Larsen and J. Miller, Trans. ASME **74**, 765 (1952).
26. R. Darolia, W.S. Walston and M.V. Nathal, *Superalloys 1996*, edited by R.D. Kissinger, D.J. Deye, D.L. Anton, A.D. Cetel, M.V. Nathal, T.M. Pollock an D.A. Woodford, The Minerals, Metals & Materials Society, Warrendale, PA, pp. 561–570 (1996).